Circuit coupled simulation of a claw–pole alternator by a temporary linearization of the 3D–FE model

E. Lange, M. van der Giet, F. Henrotte and K. Hameyer
Institute of Electrical Machines, RWTH Aachen University,
Schinkelstr. 4, D-52056 Aachen, Germany
phone: (+49)-241-80-97667, fax: (+49)-241-80-92270
E-mail: Enno.Lange@iem.rwth-aachen.de

***Abstract*— During the final stage in the design of electrical machines adequate models are required to predict the behavior at given points of operation. Due to its irreducible 3D flux path structure and the connected bridge rectifier, the claw pole generator is a challenging field–circuit coupled system. It can be solved either by permeance models, state space models or numerically strong coupled formulations within a Finite Element Analysis (FEA). Alternatively, a numerically weakly coupled method is presented in this paper. A temporary lumped parameter representation of the alternator seen from stator terminals is extracted from the Jacobian matrix of the linearized FE model. This lumped parameter representation of the machine is then incorporated into a circuit simulator based on the Modified Nodal Analysis (MNA).**

I. Introduction

OVER the past decades, various approaches have been developed to simulate field–circuit coupled problems. Among these approaches, the Magnetic Equivalent Circuit (MEC) analysis identifies the main flux paths giving a relation between winding currents and the fluxes of the machine [1]. The application of the MEC method requires a detailed knowledge of the alternator to define adequately the flux paths [2]. On the other hand, sophisticated analytical models e.g. [3] based on a 3D Fourier series representation of the airgap field have proven valuable at early design stages. Though outstandingly fast, these methods suffer in accuracy if one focuses on the optimization of power efficiency.

Undergoing significant development, the 3D FEA has been extended to cope with voltage fed coils as an integral part of field–circuit coupled simulations. The time constants of the field domain usually exceed the time constants of the circuit domain by orders of magnitude. Therefore, numerically strongly coupled approaches, e.g. [4] – [6], suffer from needlessly long simulation times. Numerically weakly coupled approaches, as proposed by [7] and [8], offer good accuracy by numerically separating field and circuit domain and herewith accounting for the different time constants of each domain.

In order to further reduce the simulation time while mainting the accuracy, it is proposed in this paper to extract a temporary lumped parameter model seen from the terminals of the alternator to be incorporated into a circuit simulator. The updating of the lumped parameters, is done either on a regular basis, or on basis of an error estimator that triggers the generation of a new set of linearized data when the error of the present set exceeds a given threshold.

The proposed model is applied to a three phase claw–pole alternator and the simulation results are compared with measurements as well as with numerical results of an alternative software package.

II. Circuit representation of the claw–pole alternator

Circuit simulators are usually based on the Modified Nodal Analysis (MNA). The nonlinear equation systems are solved by the Newton–Raphson method. Depending on the choice of the state variable of the lumped parameter model of the claw–pole alternator, the following two representations of the FE–model are possible [9]:

1) State variable: current, 0^{th} order accurate expansion.
   If the current is the state variable, the voltage drop of the upper branch of the example depicted in Fig. 1 is:
$$\begin{aligned}\nu_{r,1} - \nu_{r,2} &= \partial_t \varphi\left(i(t), \Theta(t)\right) \\ &= L^{\partial}_{rs} \delta I_s + \left(\partial_\Theta \varphi_r\right) \delta\Theta.\end{aligned} \tag{1}$$
   Herein, the first term represents the current induced voltages and the second term accounts for the motion induced voltage.
2) State variable: flux, 1^{st} order accurate expansion.
   The current through the upper branch of Fig. 1 can be written as:
$$\begin{aligned}I_r &= L^{-1}_{rk} \varphi_k + \left(\partial_\varphi I\right) \delta\varphi + \left(\partial_\Theta I_r\right) \delta\Theta \\ &= L^{-1}_{rk} \varphi_k + {L^{\partial}}^{-1}_{rk} \delta\varphi + \left(\partial_{\varphi_r} T\right) \delta\Theta.\end{aligned} \tag{2}$$

As can be seen in Fig. 1, $\nu_{r,1} - \nu_{r,2}$ represents the terminal voltage of phase r, L_{rk} and L^{∂}_{rk} are the secant, respectively the tangent, inductance matrices. The phase currents are denoted

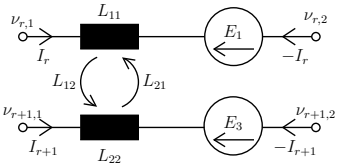

Fig. 1. Example of arbitrary lumped elements to be integrated within the circuit simulator.

I_r, the fluxes φ_r and the rotation angle Θ, respectively, the linearized state variables are δI_r, $\delta\varphi_r$ and $\delta\Theta$.

Since (2) requires the identification of both the secant and tangent inductance matrix, the current state based lumped parameter model (1) is being used in this paper.

III. Lumped Parameter Extraction

Whenever the energy of the alternator changes considerably, a new set of lumped parameters must be extracted from the FE model. For the claw–pole alternator under consideration, this happens on a regular basis as the FE–mesh needs to be modified accounting for the rotation. The extraction is based on the balance of energy of the electrical machine, as presented in [10].

A. Extraction of the inductance matrix

Let

$$M_{ij}(\mathbf{a})\ a_j = b_i, \tag{3}$$

with

$$b_i = \int_\Omega \mathbf{j}\cdot\boldsymbol{\alpha}_i = I_r \int_\Omega \mathbf{w}_r\cdot\boldsymbol{\alpha}_i = I_r W_{ir}, \tag{4}$$

be the nonlinear FE equations describing the alternator under phase and excitation currents. Herein, $\mathbf{j}$ is the current density and $\boldsymbol{\alpha}_i$ are the shape functions of the Galerkin scheme. The current shape function $\mathbf{w}_r$ of one phase of the alternator is illustrated in Fig. 2. The vector field of the current density following the threads of the winding is represented by the electric vector potential $\mathrm{rot}\,\mathbf{t} = \mathbf{j}$ calculated in advance of the coupled simulation process.

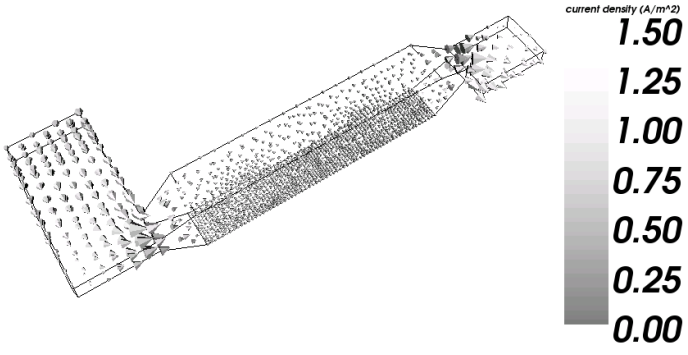

Fig. 2. Current shape function of a single stator phase.

Now, let I_r^* be the currents at time t, and $b_i^* = I_r^* W_{ir}$ the corresponding right–hand sides. Solving (3) with $b_i \equiv b_i^*$ and a fixed rotor angular position $\delta\Theta = 0$ gives a_j^* and a first order linearization around this particular solution writes

$$M_{ij}(a_j^* + \delta a_j) = M_{ij}(a_j^*)a_j^* + J_{ij}(a_j^*)\delta a_j = b_i^* + \delta b_i \tag{5}$$

with the Jacobian matrix $J_{ij} \equiv \left(\partial_{a_j} M_{ik}(a_j^*)\right) a_k^*$. Since $M_{ij}(a_j^*)a_j^* = b_i^*$, one has

$$J_{ij}(a_j^*)\ \ \delta a_j|_{\delta\Theta=0} = \delta b_i. \tag{6}$$

One can now repeatedly solve (6) with the right-hand sides $\delta b_i = \delta I_r\, W_{ir}$ obtained by perturbating one after the other m phase currents I_r and obtain m solution vectors for $\delta a_j|_{\delta\Theta=0}$. Since (6) is linear, the magnitude of the perturbations δI_r is arbitrary. One can so define by inspection the tangent inductance matrix L_{rs}^∂ of the electrical machine seen from terminals as

$$\begin{aligned}\delta\varphi_r|_{\delta\Theta=0} &= W_{rj}\ \ \delta a_j|_{\delta\Theta=0} \\ &= W_{rj}J_{ji}^{-1}(a_j^*)W_{is}\ \delta I_s, \equiv L_{rs}^\partial\ \delta I_s\end{aligned} \tag{7}$$

with

$$L_{rs}^\partial = W_{rj}J_{ji}^{-1}(a_j^*)W_{is}. \tag{8}$$

Similarly, one can identify the secant inductance matrix L_{rs} and by solving (3) repeatedly with linearly independent phase currents I_r to obtain

$$\varphi_r = W_{rj}\ a_j = W_{rj}M_{ji}^{-1}(a_j^*)W_{is}\ I_s \equiv L_{rs}\ I_s \tag{9}$$

with

$$L_{rs} = W_{rj}M_{ji}^{-1}(a_j^*)W_{is}. \tag{10}$$

It is practical for these identifications to use a solver capable of efficiently dealing with multiple right–hand sides.

B. Extraction of the motion induced voltage

One can now complement (7) to account for the electromotive force (emf):

$$\delta\varphi_r = L_{rs}^\partial\delta I_s + E_r\delta\Theta \tag{11}$$

with $E_r \equiv \partial_\Theta\varphi_r$. The direct computation of the Θ derivative requires to slightly shift the rotor, remesh, solve the FE problem, evaluate new fluxes and calculate a finite difference. In order to avoid this tedious process, one can again call on the energy principles. One has

$$E_r = \partial_\Theta\varphi_r = \partial_\Theta\partial_{I_r}\Psi_M = \partial_{I_r}\partial_\Theta\Psi_M = \partial_{I_r}T \tag{12}$$

where T is the torque and Ψ_M is the magnetic energy of the system. During the identification process described above, it is thus easy to calculate additionally the torque corresponding to the perturbed solutions $\delta a_j|_{\delta\Theta=0}$, and to evaluate the motion induced voltage E_r of each phase as the variation of torque with the perturbation of the corresponding phase current I_r.

Beware however that, as the torque is a nonlinear function of the fields, the perturbations needs in this case be small. Because of the linearity of (6), one may scale the perturbation currents in (12) which yields:

$$E_r = \frac{T(a_j^*) - T(a_j^* + \lambda\delta a_j|_{\delta\Theta=0})}{\lambda\delta I_r} \text{ with } \lambda = \kappa\frac{||a_j^*||_2}{||\delta a_j||_2}. \tag{13}$$

Herein, the scale factor is chosen between $0.01 \leq \kappa \leq 0.05$. Both the direct calculation of the Θ derivative by finite differences as well as the proposed energy–based approach (13) are implemented.

IV. Transient Coupling Scheme

The numerically independent solution process of the circuit and the field problem requires a time stepping scheme synchronizing the MNA and the FEA. A basic scheme is presented in Fig. 3. Herein, the time step width ΔT_{FE} of the FE–system is constant as already mentioned in Sec. III. By starting the simulation, the initial values of the tangent inductance matrix $L_{rs}^{\partial 0}$ and the induced voltages E_r^0 are calculated by a magnetostatic FEA and (1) is incorporated into the equation system of the circuit simulator. If the circuit simulator reaches $t >= t_{FE}^{k-1} + \Delta T_{FE}$, a new set of phase currents is imposed on the magnetostatic FE–system yielding an updated tangent inductance matrix $L_{rs}^{\partial k}$ and induced voltages E_r^k. This scheme accounts for an adaptive time stepping circuit simulator. Thus, the time step width of the circuit simulator can be adapted according to the topological changes in the external circuit caused by e.g. switching semi–conductor components.

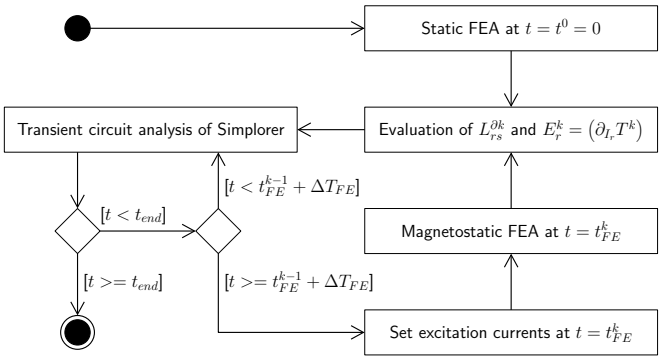

Fig. 3. Flowchart of the transient coupled simulation with static time stepping.

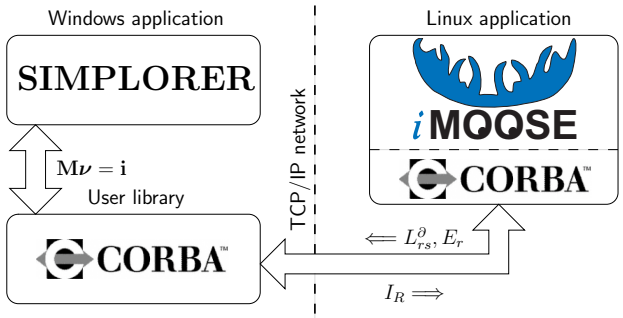

Fig. 4. Simulation infrastructure communicating via the CORBA standard.

V. Realization of Coupling

Any circuit simulator in combination with a magnetostatic FE–solver can be used provided both packages have proper interface capabilities. In this work, the circuit simulator Simplorer [11] and the in–house FE–library *i*MOOSE [12] have been used. Simplorer provides a C–Interface giving access to different stages of the time stepping scheme. Since the FE–package *i*MOOSE is written in C++, the package is flexible and can be linked to any given library.

For the field and circuit simulations run on different operating systems, and in order to avoid tedious and error–prone data exchange via files, a network based data exchange has been implemented. To reduce the implementation effort to a minimum while preserving maximum flexibility, the communication is based on the free implementation omniORB [13] of the CORBA[1] standard. The CORBA standard defines a platform independent interface definition language, by which remote procedure calls are being made transparent to the

[1]CORBA® is a registered trademark and the CORBA Logo™ is a trademark of the Object Management Group, Inc.

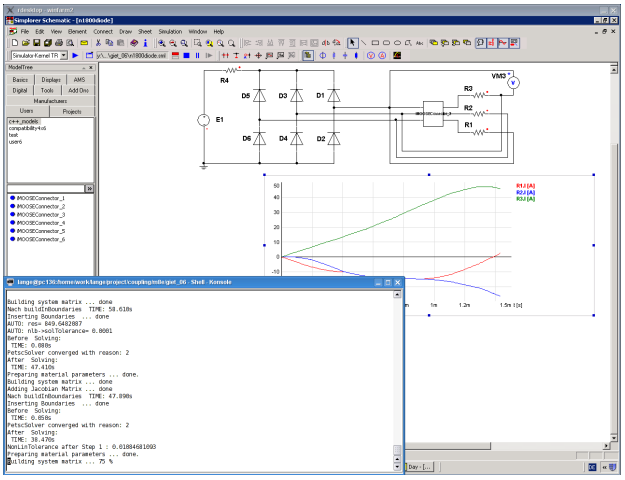

Fig. 5. Screenshot showing both the circuit simulator Simplorer in the background and the active FE-solver in the foreground.

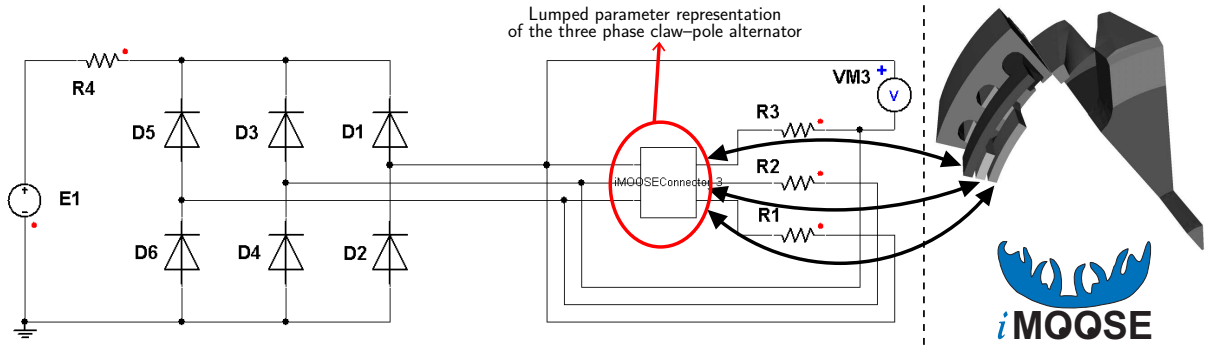

Fig. 6. Application of the proposed coupling: three phase claw–pole alternator connected to a rectifier working on a constant voltage source.

TABLE I

OVERVIEW OF THE NUMERICAL APPROACHES CHOSEN TO SIMULATE THE CLAW–POLE ALTERNATOR.

	Simulation approach	Comment
a)	*i*MOOSE $\partial_\Theta \varphi_r$	The induced voltages are calculated by finite differences similar to postprocessing.
b)	*i*MOOSE $\partial_{I_r} M$	The induced voltages are calculated by the variational approach as proposed in III-B.
c)	JMAG	Commercial software package. Implementation and exact approach unknown.

TABLE II

COMPARISON OF THE MEAN OUTPUT CURRENTS OF THE CLAW–POLE ALTERNATOR.

rotation speed	measured	*i*MOOSE $\partial_\Theta \varphi_r$	*i*MOOSE $\partial_{I_r} M$	JMAG
1500 rpm	45.73 A	58.80 A	65.03 A	80.04 A
1800 rpm	79.09 A	84.30 A	97.79 A	105.78 A
3000 rpm	128.76 A	145.18 A	139.12 A	131.80 A
6000 rpm	149.01 A	194.93 A	156.95 A	n.a.

program designer. Thereby, the program designer need not to worry about the implementation of the complete network stack.

The basic implementation is outlined in Fig. 4. Simplorer is extended by a user library which incorporates the extracted lumped parameters L_{rs}^{∂} and E_r from *i*MOOSE into the equation system of Simplorer. In turn, the actual phase currents I_r are submitted to *i*MOOSE along with a set of control parameters. All communication is done via the standard network. A screenshot showing both simulators running in parallel is shown in Fig. 5. The text interface of *i*MOOSE in the foreground gives information about the progress of FE solvings, and in the background, the simulated current waveforms are displayed in real time.

VI. APPLICATION OF COUPLING

The proposed coupling method is validated on a three phase claw–pole alternator which is connected via a B6–bridge D1–D6 to the constant voltage source E1 representing the battery in series with the resistance R4, Fig. 6. The winding resistances are labelled R1 to R3. The excitation current is assumed to be constant in this simulation, and concerns thus only the FE–system.

The inverter, whose topology is given by Fig. 6, is simulated with the emf calculated both by finite differences and by the energy approach (Sec. III-B). Additionally, the software package JMAG [14] is used as listed in Tab. I.

The alternator is inspected at different rotation speeds according to Tab. II, which shows the mean output currents of the alternator to charge the battery. Due to license issues the simulation with JMAG at 6000 rpm could not be carried out. The simulated and measured output currents are shown in Fig. 7. While implementation a) performs well at low rotation speeds, the simulated current for the highest speed clearly exceeds the measurements. Implementation b) appears to have a small offset compared to the measurement. The implementation c) performs worst at low rotation speeds but simulates the output current very accurately at medium rotation speeds. The relative error is shown in Tab. III as well as in Fig. 8.

Due to its fragile nature, implementation a) is unfavorable.

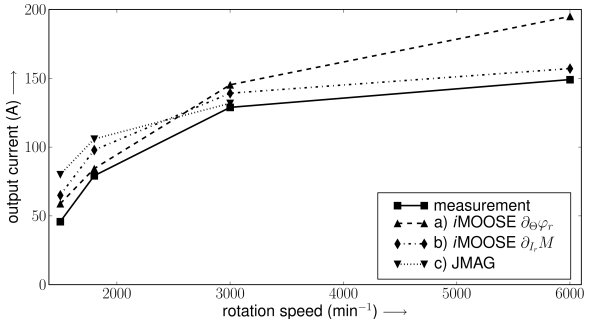

Fig. 7. Comparison of the mean output currents of the claw–pole alternator.

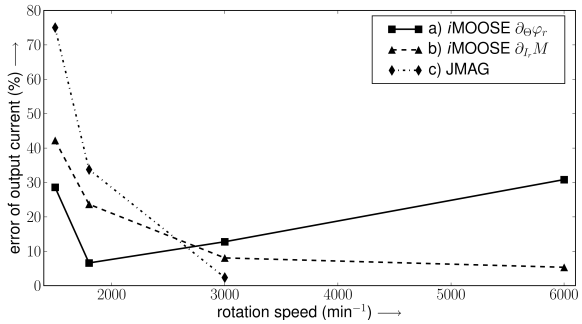

Fig. 8. Relative deviation of output current through the battery E1.

TABLE III
RELATIVE ERROR OF THE OUTPUT CURRENT.

rotation speed	*i*MOOSE $\partial_\Theta \varphi_r$	*i*MOOSE $\partial_{I_r} M$	JMAG
1500 rpm	29 %	42 %	75 %
1800 rpm	7 %	24 %	34 %
3000 rpm	13 %	8 %	2 %
6000 rpm	31 %	5 %	n.a.

The calculated induced voltage is very sensible to the chosen shift of the rotor. The offset of the implementation b) might stem from the calculation of the torque by the Maxwell stress tensor. A verification and comparison with different approaches of the calculation of the torque will provide useful additional information. All simulations deliver an output current higher than the measured one.

The phase and the output current waveforms simulated by implementation b) are depicted in Fig. 9. The flux density of the modeled claws is illustrated in Fig. 10.

VII. Discussion

The numerically weak coupling as proposed in sections II–III is applicable to simulate complex three dimensional field–circuit problems such as the claw–pole alternator. Two

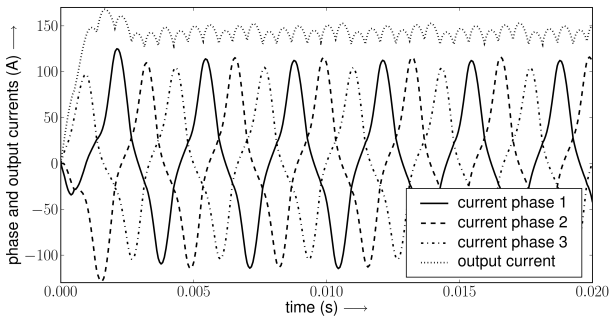

Fig. 9. Phase and output current waveforms of the alternator.

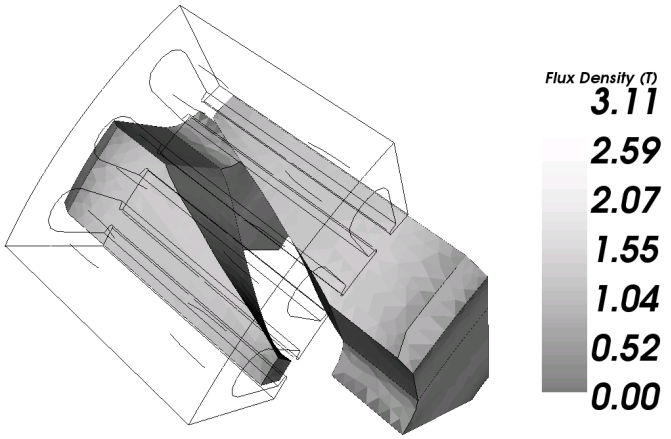

Fig. 10. Midvalue of flux density at $n = 1500\,\mathrm{rpm}$ with an excitation of $I_f = 1760\,\mathrm{Aturns}$.

approaches to calculate the motion induced voltages are implemented. Despite the good accordance between simulated and measured currents, the energy based approach is numerically stable. Though the calculation of the torque is crucial for this approach, it appears to be more reliable than the calculation of the emf by finite differences. Further investigations on the calculation of the torque are expected to give more information about the offset in the simulated mean output current.

The communication between Simplorer and *i*MOOSE via network avoids error prone file locking mechanisms necessary for synchronizing the solution process and additionally bridges the different operating systems. Furthermore, the weak coupling reduces the computation time compared to numerically strongly coupled approaches providing good results. During a standard simulation cycle the circuit simulator performs 10 times more transient steps before a new FE extraction is calculated. Thus, compared to numerically strongly coupled approaches a great saving of time is achieved.

VIII. Conclusion

In this paper, a transient field–circuit coupling based on the temporary lumped parameter representation of the FE model is presented. A transient time stepping scheme has been introduced and implemented to interconnect the circuit simulator Simplorer and the FE–package *i*MOOSE. The method has been applied to simulate a three phase claw–pole alternator connected to a B6 rectifier. The numerical results are in good accordance with measurements. The proposed method performs significantly less time consuming than numerically strongly coupled approaches.

Further research will be performed on the calculation of torque and emf, alternative circuit simulators and on advanced time stepping algorithms based on a priori and posteriori error estimations.

REFERENCES

[1] M. Hecquet, and P. Brochet, "Modeling of a claw–pole alternator using permeance network coupled with electric circuits", *IEEE Transactions on Magnetics*, vol. 31, pp. 2131–2134, May 1995.

[2] V. Ostovic, J.M. Miller, V. Garg, R.D. Schultz, and S. Swales, "A magnetic equivalent circuit based performance computation of a Lundell alternator", *IEEE Transaction on Industry Applications*, vol. 35, pp. 825–830, July/August 1999.

[3] H. Bai, S. Pekarek, J. Tichenor, W. Eversmann, D. Buening, G. Holbrok, M. Hull, R. Krefta, and S. Shields, "Analytical Derivation of a Coupled–Circuit Model of a Claw–Pole Alternator With Concentrated Stator Windings", *IEEE Transactions on Energy Conversion*, vol. 17, no. 1, pp. 32–38, March 2002.

[4] T. Dreher, and Gérard Meunier, "3D Line Current Model of Coils and External Circuits", *IEEE Transactions on Magnetics*, vol. 31, no. 3, May 1995.

[5] P.J. Leonard, and H. C. Lai, "Treatment of Symmetry in Three Dimensional Finite Element Models of Machines Coupled to External Circuits", *IEEE Transactions on Energy Conversion*, vol. 14, no. 4, December 1999.

[6] A. Canova, M. Ottella, and D. Rodger, "Coupled Field–Circuit Approach to 3D FEM Analysis of Electromechanical Devices", *Proceedings of the 9th Int. Conf. on Electrical Machines and Drives*, pp. 71–75, 1999.

[7] P. Zhou, W. N. Fu, D. Lin, S. Stanton, and Z. J. Cendes, "Numerical Modeling of Magnetic Devices", *IEEE Transactions on Magnetics*, vol. 40, pp. 1803–1809, July 2004.

[8] P. Zhou, D. Lin, W. N. Fu, B. Ionescu, and Z. J. Cendes, "A General Cosimulation Approach for Coupled Field–Circuit Problems", *IEEE Transactions on Magnetics*, vol. 42, no. 4, pp. 1051-1054, April 2006.

[9] N. A. Demerdash and T. W. Fello, "Electric Machinery Parameters and Torques by Current and Energy Perturbations from Field Computations – Part I: Theory and Formulation", *IEEE Transactions on Energy Conversion*, vol. 14, no. 4, pp. 1507–1513, December 1999.

[10] F. Henrotte and K. Hameyer, "The Structure of EM Energy Flows in Continuous Media", *IEEE Transactions on Magnetics*, vol. 42, no. 4, pp. 903-906, April 2006.

[11] Ansoft Corporation, "Simplorer", *http://www.ansoft.com*, [online], visited on May 9th, 2008.

[12] G. Arians, T. Bauer, C. Kaehler, W. Mai, C. Monzel, D. van Riesen and C. Schlensok, "Innovative modern object–oriented solving environment – iMOOSE", *http://www.imoose.de*, [online], visited on February 14th, 2008.

[13] Duncan Grisby, Apasphere Ltd, "omniORB – a robust high performance CORBA ORB for C++ and Python", *http://omniorb.sourceforge.net*, [online], visited on July 14th, 2008.

[14] JRI Solutions, Ltd., "JMAG",*http://www.jri.co.jp/pro-eng/jmag/e/jmg/*, [online], visited on July 11th, 2008.